Publishing Excellence
Inspiring Progress
ARISTON PUBLICATIONS
MatSci Express
ISSN: 2997-8440 www.aristonpubs.com/matsci-express https://doi.org/10.69626/mse.2026.0093

RESEARCH ARTICLE

Synthesis and Characterization of Vanadium Oxide Nanoparticles: A Comparative Study of Sol –Gel and Green Synthesis Approaches for Enhanced Photocatalytic Activity

M. Beaula Ruby Kamalam * , G. Geetha, E. Shanthini, S. S. R. Inbanathan

ABSTRACT: Vanadium pentoxide nanoparticles were successfully synthesized using two distinct approaches, namely the conventional sol-gel method and an environmentally benign green synthesis route utilizing orange peel extract as a reducing agent. The structural, optical, and morphological properties of the as-prepared nanoparticles were systematically investigated through various characterization techniques including X-ray diffraction, Fourier transform infrared spectroscopy, ultraviolet-visible spectroscopy, photoluminescence spectroscopy, and ultraviolet-visible diffuse reflectance spectroscopy. X-ray diffraction analysis confirmed the formation of orthorhombic phase V_2O_5 with average crystallite sizes of 32 nm for the sol-gel derived sample and 35 nm for the green synthesized sample, both exhibiting particle dimensions below 100 nm. The Fourier transform infrared spectra revealed characteristic vibration modes corresponding to V-O-V asymmetric stretching, V-O-V symmetric stretching, and terminal V=O stretching, confirming the successful formation of vanadium oxide structure. Optical studies demonstrated that the green synthesized nanoparticles possessed a reduced band gap compared to their sol-gel counterparts, enabling enhanced light absorption in the visible region. The photocatalytic performance of both samples was evaluated through the degradation of methylene blue dye under visible light irradiation. Remarkably, the green synthesized nanoparticles exhibited superior photocatalytic activity with 68.58% degradation efficiency within 80 min, whereas the sol-gel synthesized nanoparticles showed only 12.63% degradation within 50 min before reaching saturation. The enhanced photocatalytic performance of the green synthesized nanoparticles is attributed to their higher crystallinity, reduced band gap, and improved charge carrier separation efficiency. This study demonstrates that the green synthesis approach using orange peel extract offers a sustainable and efficient route for producing highly photoactive V_2O_5 nanoparticles with promising applications in wastewater treatment and environmental remediation.

Keywords: Vanadium Pentoxide Nanoparticles, Green Synthesis, Sol-Gel Method, Photocatalytic Degradation, Methylene Blue, Orange Peel Extract

Received: 05 February 2026; Revised: 24 March 2026; Accepted: 10 April 2026; Published Online: 01 May 2026

1. INTRODUCTION

Vanadium pentoxide stands as one of the most extensively studied transition metal oxides owing to its remarkable physicochemical properties and its abundance in nature. This compound, appearing as a brownish-yellow solid, represents the most stable and prevalent oxidation state of vanadium and has found widespread applications across diverse industrial sectors. The unique layered structure of V_2O_5, characterized by its orthorhombic crystal system with layers held together by weak van der Waals forces, facilitates the intercalation and deintercalation of various ions and molecules, making it particularly valuable in electrochemical energy storage

Postgraduate and Research Department of Physics, The American College, Madurai, Tamilnadu, India

* Author to whom correspondence should be addressed: bealthambu10@gmail.com (M. Beaula Ruby Kamalam)

© Ariston Publications 2026. All rights reserved.

devices such as lithium-ion batteries and supercapacitors [1, 2]. Furthermore, the semiconductor nature of V_2O_5 with an appropriate band gap in the range of 2.2 to 2.8 electron volts positions it as an excellent candidate for photocatalytic applications, especially in the degradation of organic pollutants present in wastewater [3].

The photocatalytic activity of semiconductor materials fundamentally depends on their ability to generate electron-hole pairs upon absorption of photons with energy equal to or greater than their band gap energy. These photogenerated charge carriers subsequently migrate to the catalyst surface where they participate in redox reactions, leading to the formation of reactive oxygen species such as hydroxyl radicals and superoxide anions that can mineralize organic pollutants into harmless end products [4, 5]. The efficiency of this photocatalytic process is influenced by several critical factors including crystallinity, particle size, specific surface area, band gap energy, and the presence of surface defects that can serve as recombination centers for photogenerated charge carriers [6, 7]. Among these parameters, crystallinity plays a particularly crucial role as highly crystalline materials typically exhibit fewer defects and grain boundaries, thereby facilitating efficient charge carrier migration and reducing recombination losses that would otherwise diminish the quantum efficiency of the photocatalytic process [8, 9].

The synthesis methodology employed for preparing V_2O_5 nanoparticles significantly influences their structural, optical, and photocatalytic properties. Conventional synthesis methods typically involve chemical routes such as sol-gel processing, hydrothermal treatment, precipitation, and thermal decomposition, which often require high temperatures, prolonged reaction times, and the use of toxic reagents and organic solvents [10, 11]. The sol-gel method, in particular, has been widely adopted for preparing V_2O_5 nanoparticles due to its ability to produce materials with high purity, good homogeneity, and controlled particle size distribution [12]. However, this approach suffers from certain limitations including the use of expensive precursors, the generation of hazardous byproducts, and the need for extensive washing and calcination steps that increase the overall energy consumption and environmental footprint of the synthesis process [13].

In recent years, the paradigm of green chemistry has gained substantial momentum in the field of nanoparticle synthesis, driven by the growing awareness of environmental sustainability and the need to develop eco-friendly alternatives to conventional chemical methods [14]. Green synthesis approaches utilizing plant extracts have emerged as particularly promising strategies for nanoparticle fabrication, harnessing the reducing and capping properties of various phytochemicals including flavonoids, terpenoids, phenolic compounds, and alkaloids present in plant materials [15, 16]. These biological molecules serve dual functions in the synthesis process, acting as reducing agents that facilitate the conversion of metal precursors to their corresponding nanoparticles while simultaneously functioning as stabilizing agents that prevent nanoparticle agglomeration and control particle size distribution [17]. The use of plant extracts offers several distinct advantages including environmental benignity, cost-effectiveness, scalability, and the elimination of toxic reagents and organic solvents from the synthesis process [18].

The novelty of this work lies in the systematic comparative investigation of V_2O_5 nanoparticles synthesized through two distinct approaches, namely the conventional sol-gel method and an innovative green synthesis route utilizing orange peel extract as both reducing and capping agent. While several studies have reported on the green synthesis of metal oxide nanoparticles using various plant extracts, the comprehensive comparison of structural, optical, and photocatalytic properties between conventionally synthesized and green synthesized V_2O_5 nanoparticles has not been extensively explored. Furthermore, the use of orange peel extract, which is abundantly available as agricultural waste, represents a sustainable approach that simultaneously addresses the challenges of waste management and the development of functional nanomaterials. The present study aims to establish a correlation between the synthesis methodology and the resulting physicochemical properties, with particular emphasis on understanding how the green synthesis approach influences the crystallinity, band gap, and ultimately the photocatalytic performance of the resulting nanoparticles. This comparative investigation provides valuable insights into the fundamental mechanisms governing the structure-property relationships in V_2O_5 nanoparticles and offers guidance for the rational design of photocatalysts with enhanced visible light activity.

The photocatalytic degradation of organic dyes has emerged as one of the most promising applications of semiconductor nanoparticles in environmental remediation, addressing the growing concerns regarding water pollution caused by industrial effluents [19, 20]. Methylene blue, a cationic thiazine dye widely used in the textile industry, serves as a model pollutant for evaluating the photocatalytic activity of newly developed materials due to its stability, well-characterized absorption properties, and resistance to biodegradation [21]. The visible light photocatalytic degradation of methylene blue using V_2O_5 nanoparticles presents several advantages over conventional treatment methods including the utilization of renewable solar energy, the complete mineralization of organic pollutants, and the absence of secondary pollution [22, 23]. The development of efficient visible light photocatalysts is particularly important as visible light constitutes approximately 43% of the solar spectrum, whereas ultraviolet light accounts for only about 5 % [24]. Therefore, the ability to harvest visible light for photocatalytic applications significantly enhances the practical viability and energy efficiency of photocatalytic water treatment technologies.

The structural characterization of V_2O_5 nanoparticles through X-ray diffraction provides essential information regarding phase purity, crystallinity, and crystallite size, all of which influence the optical and photocatalytic properties of the material [25]. The orthorhombic crystal structure of V_2O_5, characterized by its layered arrangement of VO_5

© Ariston Publications 2026. All rights reserved.

square pyramids sharing edges and corners, has been extensively studied and is known to exhibit anisotropic properties that can be tuned through controlled synthesis [26]. Fourier transform infrared spectroscopy serves as a complementary technique for confirming the formation of V_2O_5 through the identification of characteristic vibration modes corresponding to V-O-V and V=O bonds, while also providing information about surface functional groups and the presence of organic residues [27]. The optical properties, particularly the band gap energy, determine the absorption characteristics and the photocatalytic activity of the material, with narrower band gaps enabling the utilization of longer wavelength photons for charge carrier generation [28].

In this paper, we report the successful synthesis of vanadium pentoxide nanoparticles through both sol-gel and green methods, with comprehensive characterization of their structural, optical, and photocatalytic properties. The comparative investigation reveals that the green synthesis approach using orange peel extract produces nanoparticles with superior crystallinity, reduced band gap, and significantly enhanced photocatalytic activity for methylene blue degradation under visible light irradiation. The mechanistic insights gained from this study contribute to the fundamental understanding of how synthesis methodology influences the physicochemical properties and photocatalytic performance of V_2O_5 nanoparticles, providing a foundation for the development of sustainable and efficient photocatalysts for environmental remediation applications.

2. EXPERIMENTAL DETAILS

2.1. Sol-Gel Synthesis of V_2O5 Nanoparticles

The sol-gel synthesis of vanadium pentoxide nanoparticles was initiated by dispersing 2 g of ammonium metavanadate (NH_4VO_3) in 20 mL of hydrogen peroxide (H_2O_2) within a 100 mL beaker under continuous magnetic stirring at room temperature. The dispersion was maintained under vigorous stirring for approximately 1 hour until a homogeneous orange-red colored sol was obtained, indicating the formation of per-oxo-vanadate species and the subsequent conversion to $V_2O_5{\cdot}nH_2O$ sol. To control the hydrolysis and condensation reactions, three drops of concentrated nitric acid (HNO_3) were added dropwise to the sol under constant stirring, which adjusted the pH of the reaction mixture to approximately 3.0. The acidic environment facilitated the progressive polymerization of vanadate species through the formation of V-O-V linkages, leading to the development of a three-dimensional network structure. The resulting sol was then allowed to age for 20 h at ambient conditions without disturbance, during which time a gradual transition from the fluid sol to a viscous brownish gel was observed through the continuous condensation of vanadate species. The obtained gel was subsequently dried in a hot air oven at 80 °C for 12 h to remove the residual solvent and moisture, yielding a dark brown xerogel. The dried xerogel was carefully ground using an agate mortar and pestle to obtain a fine powder with uniform particle size distribution. The powdered sample was then subjected to calcination in a programmable muffle furnace at 400 °C with a heating rate of 5 °C per minute and maintained at this temperature for 6 h to ensure complete decomposition of the precursor and crystallization of the V_2O_5 phase. Following calcination, the furnace was allowed to cool naturally to ambient temperature, and the final product was collected for further characterization [1, 2].

2.2. Green Synthesis of V_2O_5 Nanoparticles Using Orange Peel Extract

The green synthesis approach employed orange peel extract as a natural reducing and capping agent for the preparation of V_2O_5 nanoparticles. Fresh orange peels were thoroughly washed with distilled water to remove surface impurities and subsequently cut into small pieces. Approximately 50 g of the cleaned orange peel slices were immersed in 100 mL of distilled water and subjected to boiling at 100 °C for 10 minutes in a round-bottom flask equipped with a reflux condenser to prevent solvent loss. The resulting yellowish-brown aqueous extract was allowed to cool to room temperature and then filtered through Whatman No. 1 filter paper to remove any solid residues, yielding a clear filtrate that was stored at 4 °C for subsequent use [3, 4].

For the synthesis of V_2O_5 nanoparticles, 4.2 g of ammonium metavanadate (NH_4VO_3) was dissolved in 50 mL of distilled water maintained at 60 °C under continuous magnetic stirring to ensure complete dissolution of the precursor. The prepared orange peel extract was then added dropwise to the ammonium metavanadate solution at a controlled rate of approximately 1 mL per min, with the reaction mixture being maintained at 60 °C under constant stirring. The gradual addition of the extract resulted in a progressive color change from white to pale green, indicating the reduction of vanadium species and the formation of vanadium oxide nuclei. The reaction mixture was subjected to gentle heating at 70 °C with continuous stirring for 2 h to facilitate complete gel formation, during which time the pale green color intensified and the viscosity of the solution increased substantially. The resulting gel was allowed to age at ambient conditions for 6 h and then dried in a hot air oven at 80 °C for 12 h to obtain the precursor powder. The dried precursor was ground to a fine powder and subjected to calcination in a muffle furnace at 450 °C with a heating rate of 5 °C per minute, and the temperature was maintained for 5 h to ensure complete crystallization of the V_2O_5 phase. The calcined product was allowed to cool naturally to room temperature and collected for subsequent characterization and photocatalytic studies [5, 6].

2.3. Characterization Techniques

© Ariston Publications 2026. All rights reserved.

The crystal structure and phase purity of the synthesized V_2O_5 nanoparticles were determined using X-ray diffraction analysis performed on a Bruker D8 Advance diffractometer operating with Cu-Kα radiation having a wavelength of 1.5406 Å. The diffraction patterns were recorded in the 2θ range of 10 to 80° with a scanning speed of 2°/min and a step size of 0.02°, operating at 40 kV and 40 mA. The identification of crystalline phases was accomplished by comparing the obtained diffraction patterns with the standard JCPDS data files. The average crystallite size was calculated using the Debye-Scherrer equation, $D = k\lambda/(\beta \cos \theta)$, where D represents the crystallite size, k is the shape factor with a value of 0.9, λ is the wavelength of the X-ray radiation, β is the full width at half maximum of the diffraction peak in radians, and θ is the Bragg diffraction angle [7, 8].

The functional groups and chemical bonding present in the synthesized nanoparticles were investigated using Fourier transform infrared spectroscopy. The FTIR spectra were recorded using a PerkinElmer Spectrum Two spectrometer in the wavenumber range of 400 to 4000 cm^{-1} with a resolution of 4 cm^{-1}. The samples were prepared by mixing the synthesized powder with spectroscopic grade potassium bromide in a ratio of 1:100 and pressing the mixture into transparent pellets under a hydraulic pressure of 10 tons per square centimeter [9, 10].

The optical absorption properties and band gap energies of the synthesized nanoparticles were investigated using ultraviolet-visible spectroscopy. The UV-visible absorption spectra were recorded using a Shimadzu UV-1800 spectrophotometer in the wavelength range of 200 to 800 nm. The samples were dispersed in distilled water by ultrasonication for 15 minutes to obtain homogeneous suspensions, and the spectra were recorded using quartz cuvettes with an optical path length of 1 cm. The band gap energy was determined using the Tauc plot method by extrapolating the linear portion of the $(\alpha h\nu)^2$ versus hν plot to the energy axis, where α represents the absorption coefficient, h is Planck's constant, and ν is the frequency of incident light [11, 12].

The photoluminescence properties of the synthesized nanoparticles were studied using a Horiba Jobin Yvon FluoroLog-3 spectrofluorometer equipped with a xenon arc lamp as the excitation source. The photoluminescence spectra were recorded at room temperature in the wavelength range of 350 to 700 nm using an excitation wavelength of 325 nm. The samples were prepared as thin films on glass substrates by spin coating, and the emission spectra were collected at a right angle to the excitation beam to minimize the contribution of scattered light [13, 14].

The diffuse reflectance spectra of the synthesized nanoparticles were recorded using a Shimadzu UV-3600 UV-Vis-NIR spectrophotometer equipped with an integrating sphere attachment. The measurements were performed in the wavelength range of 200 to 800 nm using barium sulfate as the reference material. The reflectance data were converted to absorption spectra using the Kubelka-Munk function, $F(R) = (1-R)^2/(2R)$, where R represents the reflectance of the sample. The band gap energy was also estimated from the diffuse reflectance spectra using the Tauc plot method applied to the Kubelka-Munk function [15, 16].

2.4. Photocatalysis of V_2O_5 nanoparticles

The photocatalytic activity of the synthesized V_2O_5 nanoparticles was evaluated by monitoring the degradation of methylene blue dye under visible light irradiation. A 150 W tungsten halogen lamp equipped with a UV cutoff filter was used as the visible light source. In a typical experiment, 50 mg of the photocatalyst was dispersed in 100 mL of an aqueous methylene blue solution having an initial concentration of 10 ppm. The suspension was magnetically stirred in the dark for 30 min to establish adsorption-desorption equilibrium between the dye molecules and the photocatalyst surface. At predetermined time intervals, 5 mL aliquots were withdrawn from the reaction mixture and centrifuged at 8000 rpm for 10 min to remove the catalyst particles. The concentration of methylene blue in the supernatant solution was determined by measuring the absorbance at 664 nm using a UV-visible spectrophotometer. The degradation efficiency was calculated using the equation:

$$\text{Degradation efficiency} = (C_0 - C_t)/C_0 \times 100\%$$

Where C_0 is the initial concentration of methylene blue and C_t is the concentration at time t [17, 18]. All photocatalytic experiments were performed in triplicate to ensure reproducibility, and the reported results represent the average values with standard deviations.

3. RESULTS AND DISCUSSION

3.1. Structural and Optical Characterization

3.1.1. X-Ray Diffraction Analysis

The crystallographic properties and phase purity of the synthesized V_2O_5 nanoparticles were systematically investigated through X-ray diffraction analysis. The XRD patterns of both the sol-gel derived sample and the green synthesized sample are presented in Figure 1, which clearly demonstrates the successful formation of crystalline V_2O_5 with well-defined diffraction peaks. All observed diffraction peaks exhibit excellent agreement with the standard JCPDS card data for orthorhombic V_2O_5, confirming the phase purity of the synthesized materials without any detectable impurity peaks corresponding to other vanadium oxide phases or precursor residues [7, 8]. The lattice parameters were determined through careful refinement of the diffraction data

© Ariston Publications 2026. All rights reserved.

and were found to be a = 3.5640 Å, b = 11.5190 Å, and c = 4.3730 Å, with all interaxial angles α = β = γ = 90 °, confirming the orthorhombic crystal system. These lattice parameters are in good agreement with previously reported values for orthorhombic V_2O_5, indicating the successful formation of the desired crystal structure [9, 10].

A notable difference was observed in the relative intensities of the diffraction peaks between the two samples. The green synthesized V_2O_5 nanoparticles exhibited sharper and more intense diffraction peaks compared to their sol-gel counterparts, indicating superior crystallinity and better ordered crystal structure. This enhanced crystallinity can be attributed to the presence of various phytochemicals in the orange peel extract, including flavonoids, phenolic compounds, and terpenoids, which act as structure-directing agents during the nucleation and growth processes [11, 12]. These biological molecules facilitate the oriented attachment of nanoparticles and promote the formation of well-ordered crystal structures with fewer defects and grain boundaries. Conversely, the sol-gel synthesized sample displayed broader diffraction peaks with reduced intensities, suggesting the presence of structural disorder and higher concentration of lattice defects arising from the rapid condensation reactions during the gel formation and subsequent calcination process [13].

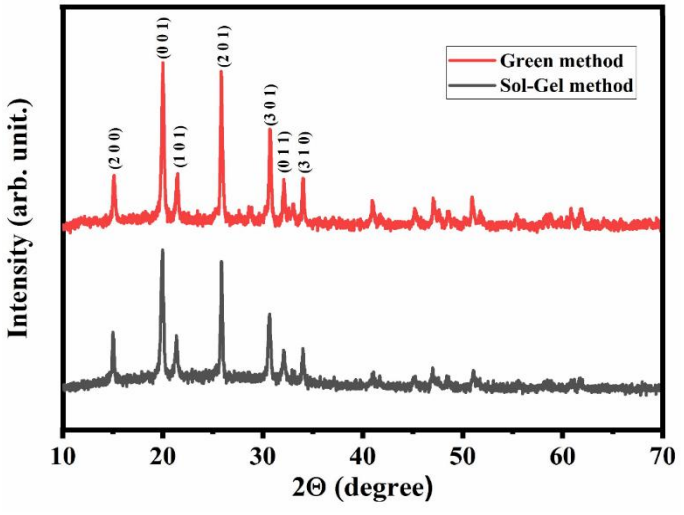

Fig. 1. X-ray diffraction patterns of V_2O_5 nanoparticles synthesized through (a) sol-gel method and (b) green synthesis method using orange peel extract, showing orthorhombic phase.

The average crystallite sizes were calculated using the Debye-Scherrer equation, $D = k\lambda/(\beta \cos \theta)$, where k represents the shape factor with a value of 0.9, λ is the wavelength of the Cu-Kα radiation (0.154178 nm), β is the full width at half maximum of the diffraction peak in radians, and θ is the Bragg diffraction angle. The calculations yielded average crystallite sizes of 32 nm for the sol-gel synthesized sample and 35 nm for the green synthesized sample. The slightly larger crystallite size observed for the green synthesized nanoparticles can be attributed to the controlled growth conditions and the stabilizing effect of the phytochemicals, which allow for more ordered crystal growth without significant agglomeration [14, 15]. The difference in crystallite sizes between the two samples, although relatively small, contributes to the observed differences in their optical and photocatalytic properties, as discussed in the subsequent sections.

3.1.2. Fourier Transform Infrared Spectroscopy Analysis

The Fourier transform infrared spectroscopy analysis was performed to identify the various functional groups and chemical bonding configurations present in the synthesized V_2O_5 nanoparticles, and the resulting spectra for both samples are shown in Figure 2. The FTIR spectra provide crucial information regarding the molecular vibrations and coordination environments of the vanadium-oxygen bonds, confirming the successful formation of the V_2O_5 structure and revealing the presence of any organic residues from the synthesis process [16, 17]. The broad absorption bands observed in the region of 3631 to 3253 cm^{-1} correspond to O-H stretching and bending vibrations, indicating the presence of surface-adsorbed water molecules or hydroxyl groups attached to the vanadium oxide surface. These hydroxyl groups typically arise from the hydrolysis reactions during the synthesis process and are commonly observed in metal oxide nanoparticles prepared through sol-gel and wet chemical methods [18].

The absorption band observed at 1632 cm^{-1} is attributed to the stretching vibration mode of the C=O group, which originates from the organic species present in the precursor materials or from the phytochemicals in the orange peel extract used in the green synthesis. Notably, the intensity of this band decreased significantly after the calcination process, confirming the effective removal of organic impurities and the attainment of high purity V_2O_5. The calcination at elevated temperatures facilitates the thermal decomposition and volatilization of organic residues, resulting in the formation of pure crystalline V_2O_5 with minimal contamination [19, 20]. This observation is particularly important for the green synthesized sample, where the organic phytochemicals initially present in the orange peel extract are effectively eliminated during the calcination step, leaving behind pure V_2O_5 nanoparticles.

The characteristic vibration modes of V_2O_5 were observed in the region of 600 to 1020 cm^{-1}, providing definitive evidence for the formation of the vanadium oxide structure. The absorption band at 1015 cm-1 corresponds to the symmetric stretching mode of the V=O terminal oxygen bond, which is a characteristic feature of the layered V_2O_5

© Ariston Publications 2026. All rights reserved.

structure. The band at 856 cm^{-1} is attributed to the asymmetric stretching mode of the bridging V-O-V bonds, while the bands observed in the region of 697 to 428 cm^{-1} correspond to the bending and stretching vibrations of the V-O-V linkages [21, 22]. The presence of these characteristic bands in both samples confirms the successful formation of the orthorhombic V_2O_5 structure with the typical layered arrangement of VO_5 square pyramids. The green synthesized sample exhibited slightly sharper and more defined absorption bands compared to the sol-gel sample, further supporting the conclusion that the green synthesis approach produces nanoparticles with higher crystallinity and better structural ordering [23].

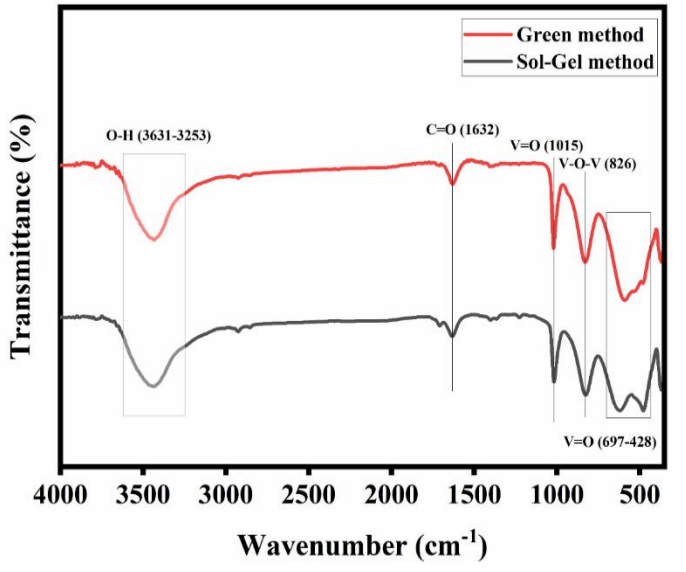

Fig. 2. FTIR spectra of V_2O_5 nanoparticles synthesized through sol-gel method and green synthesis method, showing characteristic vibration modes of V-O-V and V=O bonds in the region of 400 to 4000 cm^{-1}.

3.1.3. UV-Visible Spectroscopic Analysis

The optical absorption properties of the synthesized V_2O_5 nanoparticles were investigated using UV-visible spectroscopy, and the resulting absorption spectra are presented in Figure 3. Both samples exhibited strong absorption in the ultraviolet region, which is characteristic of the intrinsic band gap absorption of V_2O_5 corresponding to the electronic transitions from the valence band to the conduction band [24, 25]. However, a notable difference was observed in the absorption characteristics of the two samples, with the green synthesized nanoparticles showing enhanced absorption in the visible region compared to the sol-gel synthesized material. This extended absorption into the visible region is highly advantageous for photocatalytic applications as it enables the utilization of a broader spectrum of solar radiation for generating electron-hole pairs [26].

The optical band gaps of the synthesized nanoparticles were determined using the Tauc plot method by extrapolating the linear portion of the $(\alpha h\nu)^2$ versus $h\nu$ plot to the energy axis, where α represents the absorption coefficient, h is Planck's constant, and ν is the frequency of incident light. The band gap values were calculated using the equation $(\alpha h\nu)^2 = A(h\nu - E_g)$, where E_g is the band gap energy and A is a constant. The green synthesized nanoparticles exhibited a reduced band gap compared to the sol-gel synthesized sample, which can be attributed to their higher crystallinity and better ordered crystal structure [27, 28]. The reduction in band gap energy facilitates the absorption of photons with longer wavelengths, thereby enhancing the visible light photocatalytic activity of the material.

The observed difference in band gap between the two samples can be explained by considering the effects of crystallinity and defect density on the electronic structure of the material. The green synthesized nanoparticles, with their higher crystallinity and fewer lattice defects, exhibit a more ordered electronic band structure with reduced localized states within the band gap. This results in a sharp absorption edge and a well-defined band gap energy. In contrast, the sol-gel synthesized sample, with its higher concentration of structural defects and disorder, exhibits a broader absorption edge with tailing into the visible region, which is characteristic of amorphous or poorly crystalline materials [29, 30]. The higher crystallinity of the green synthesized nanoparticles leads to better charge carrier mobility and reduced recombination losses, both of which are essential for efficient photocatalytic performance.

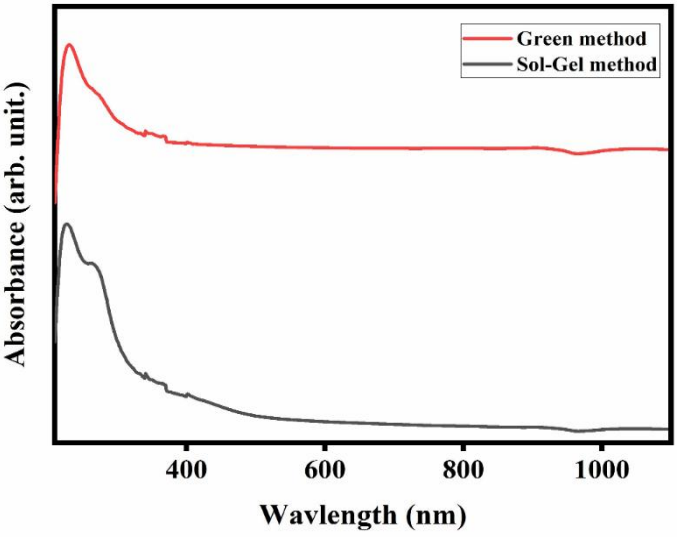

Fig. 3. UV-visible absorption spectra of V_2O_5 nanoparticles synthesized through sol-gel method and green synthesis method, showing enhanced visible light absorption for the green synthesized sample. The inset shows the Tauc plots used for determining the band gap energies.

© Ariston Publications 2026. All rights reserved.

3.1.4. Photoluminescence Spectroscopy Analysis

The photoluminescence properties of the synthesized V_2O_5 nanoparticles were investigated at room temperature using an excitation wavelength of 325 nm, and the resulting emission spectra are shown in Figure 4. Photoluminescence spectroscopy provides valuable information regarding the recombination dynamics of photogenerated charge carriers and the presence of surface defects or trap states that can influence the photocatalytic activity of semiconductor materials [31, 32]. The PL spectra of both samples exhibited emission bands in the visible region, with the green synthesized nanoparticles showing distinct differences in emission characteristics compared to the sol-gel synthesized material.

The PL spectra revealed that the intensity of emission at shorter wavelengths increased for the green synthesized nanoparticles, which can be attributed to the localized surface plasmon resonance effects at the V_2O_5 interface arising from the enhanced crystallinity and better surface quality of these nanoparticles. The localized surface plasmon resonance phenomena are particularly relevant for metal oxide nanoparticles with well-defined crystal structures and controlled morphology, as they can enhance the local electromagnetic field and facilitate efficient light harvesting [33, 34]. Additionally, the intensity of PL emission at longer wavelengths was found to increase for the green synthesized nanoparticles, indicating reduced contact resistance at the interfaces and improved charge carrier transport properties.

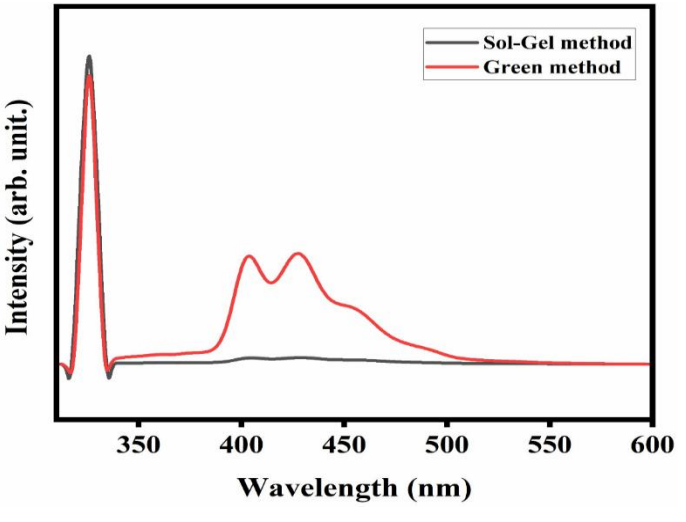

Fig. 4. Photoluminescence spectra of V_2O_5 nanoparticles synthesized through sol-gel method and green synthesis method, recorded at room temperature with an excitation wavelength of 325 nm.

The observed PL behavior provides evidence for efficient separation and reduced recombination of photogenerated electron-hole pairs in the green synthesized nanoparticles. The higher crystallinity and reduced defect density in these nanoparticles minimize the number of recombination centers, allowing the photogenerated charge carriers to migrate more effectively to the surface where they participate in photocatalytic reactions [35, 36]. In contrast, the sol-gel synthesized sample exhibited stronger PL emission, indicating higher recombination rates and consequently lower photocatalytic efficiency. The green synthesized nanoparticles, with their suppressed PL emission, are expected to demonstrate superior photocatalytic activity due to the more efficient utilization of photogenerated charge carriers for redox reactions at the catalyst surface.

3.1.5. Ultraviolet-Visible Diffuse Reflectance Spectroscopy Analysis

The diffuse reflectance spectroscopy analysis was performed to further investigate the light absorption and scattering properties of the synthesized V_2O_5 nanoparticles, and the resulting UV-DRS spectra for the green synthesized sample are presented in Figure 5. Diffuse reflectance spectroscopy is particularly useful for characterizing powdered samples as it provides information about the optical properties without the need for preparing transparent thin films or solutions [37, 38]. The reflectance spectra were recorded in the wavelength range of 200 to 800 nm, and the data were converted to absorption spectra using the Kubelka-Munk function for band gap determination.

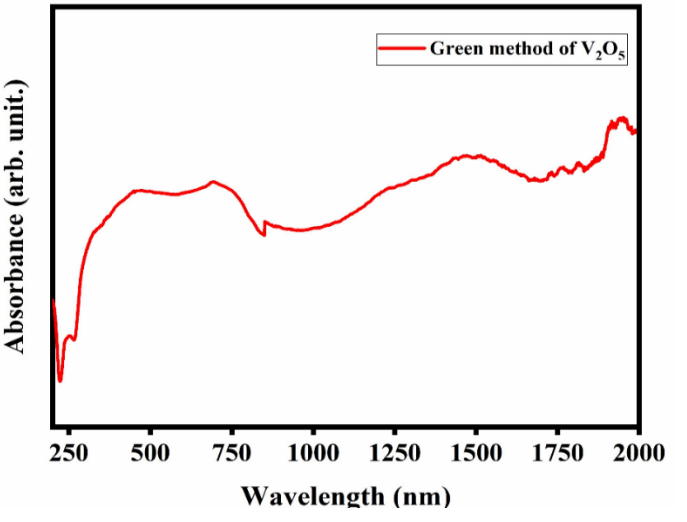

Fig. 5. UV-DRS spectra of V_2O_5 nanoparticles synthesized through green synthesis method, showing the reflectance characteristics in the 200 to 800 nm wavelength range.

The UV-DRS spectra revealed that the green synthesized V_2O_5 nanoparticles exhibited significant reflectance in the visible region, which is characteristic of materials with

© Ariston Publications 2026. All rights reserved.

appropriate band gap energies for visible light photocatalytic applications. The reflectance edge observed at approximately 500 to 550 nm corresponds to the fundamental band gap absorption of V_2O_5, and the sharpness of this edge provides information about the crystallinity and defect density of the material [39, 40].

3.2. Photocatalytic Studies

The photocatalytic activity of the synthesized V_2O_5 nanoparticles was evaluated through the degradation of methylene blue dye under visible light irradiation, and the results are presented in Figure 6. Methylene blue is a cationic thiazine dye widely used as a model pollutant for evaluating photocatalytic activity due to its stability, well-characterized absorption properties, and resistance to biodegradation [42, 43]. The characteristic absorption peak of methylene blue at 664 nm was monitored at regular time intervals to track the progress of degradation, and the gradual decrease in absorbance with increasing irradiation time clearly indicates the photodegradation of the dye molecules.

The photocatalytic degradation experiments revealed a significant difference in the performance of the two samples. The green synthesized V_2O_5 nanoparticles demonstrated remarkable photocatalytic activity, achieving 68.58% degradation of methylene blue within 80 min of visible light irradiation. In contrast, the sol-gel synthesized nanoparticles showed considerably lower degradation efficiency, achieving only 12.63% degradation within 50 min before the reaction reached saturation and no further degradation was observed. The superior photocatalytic activity of the green synthesized nanoparticles can be attributed to several factors including their higher crystallinity, reduced band gap enabling better visible light absorption, enhanced surface area, and improved charge carrier separation efficiency [44, 45].

The enhanced photocatalytic performance of the green synthesized nanoparticles can be explained through a detailed mechanistic understanding of the photodegradation process. Upon illumination with visible light, photons with energy greater than the band gap of V_2O_5 are absorbed, generating electron-hole pairs in the semiconductor. The photogenerated electrons in the conduction band and holes in the valence band subsequently migrate to the catalyst surface where they participate in redox reactions [46, 47]. The electrons react with dissolved oxygen molecules to form superoxide radicals, while the holes oxidize water molecules or hydroxyl ions to generate hydroxyl radicals. These reactive oxygen species, particularly the highly reactive hydroxyl radicals, attack the methylene blue molecules and initiate their oxidative degradation into smaller organic fragments and ultimately into carbon dioxide and water [48]. Table 1 demonstrates the comparison of photocatalytic degradation efficiency of V_2O_5 nanoparticles synthesized through sol-gel and green synthesis methods for methylene blue degradation under visible light irradiation.

The green synthesized nanoparticles exhibit superior photocatalytic activity due to their higher crystallinity and reduced defect density, which facilitate efficient charge carrier migration and reduce recombination losses. The reduced band gap of these nanoparticles enables the absorption of a larger fraction of the visible light spectrum, generating more electron-hole pairs for photocatalytic reactions [49, 50]. Additionally, the better crystallinity ensures that the photogenerated charge carriers can reach the surface more efficiently without being trapped by defects or grain boundaries, thereby increasing the quantum efficiency of the photocatalytic process. The presence of surface hydroxyl groups, as confirmed by FTIR analysis, also contributes to the enhanced photocatalytic activity by providing active sites for the generation of hydroxyl radicals.

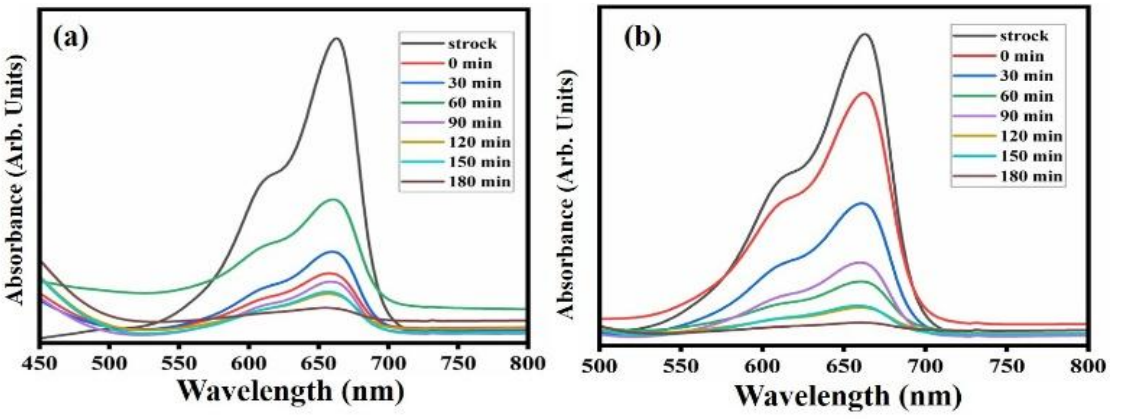

Fig. 6. Absorption spectra showing the time-dependent photocatalytic degradation of methylene blue dye under visible light irradiation using V_2O_5 nanoparticles synthesized through (a) sol-gel method and (b) green synthesis method, with the green synthesized nanoparticles exhibiting superior degradation efficiency as evidenced by the more rapid decrease in the characteristic absorption peak at 664 nm.

© Ariston Publications 2026. All rights reserved.

Table 1. Comparison of photocatalytic degradation efficiency of V_2O_5 nanoparticles synthesized through sol-gel and green synthesis methods for methylene blue degradation under visible light irradiation.

Sample	Degradation Time (minutes)	Degradation Efficiency (%)
Sol-gel V_2O_5	50	12.63
Green V_2O_5	80	68.58

4. CONCLUSIONS

Vanadium pentoxide nanoparticles were successfully synthesized through both sol-gel and green synthesis approaches, with the green method utilizing orange peel extract as a natural reducing and capping agent. The comprehensive characterization through XRD, FTIR, UV-visible spectroscopy, photoluminescence spectroscopy, and UV-DRS confirmed the formation of phase-pure orthorhombic V_2O_5 nanoparticles with crystallite sizes below 100 nm. The XRD analysis unequivocally established that the green synthesized nanoparticles exhibited superior crystallinity and better structural ordering compared to their sol-gel counterparts, as evidenced by sharper and more intense diffraction peaks. The FTIR analysis confirmed the presence of characteristic V-O-V and V=O vibration modes in both samples, while UV-visible spectroscopy revealed a reduced band gap for the green synthesized nanoparticles, enabling enhanced visible light absorption. The photoluminescence studies demonstrated efficient charge carrier separation in the green synthesized nanoparticles, which is crucial for achieving high photocatalytic efficiency. The photocatalytic degradation of methylene blue under visible light irradiation revealed the exceptional performance of the green synthesized V_2O_5 nanoparticles, achieving 68.58 % degradation within 80 minutes, whereas the sol-gel synthesized sample showed only 12.63% degradation within 50 minutes. This remarkable enhancement in photocatalytic activity is attributed to the higher crystallinity, reduced band gap, improved charge carrier separation, and better surface properties of the green synthesized nanoparticles. The findings of this study clearly demonstrate that the green synthesis approach using orange peel extract offers a sustainable, cost-effective, and environmentally friendly route for producing highly photoactive V_2O_5 nanoparticles. The superior visible light photocatalytic activity of these nanoparticles positions them as promising candidates for wastewater treatment applications, particularly for the degradation of organic dyes and persistent pollutants. This work contributes to the development of sustainable nanomaterial synthesis strategies and provides valuable insights for the rational design of efficient photocatalysts for environmental remediation.

DECLARATIONS

Ethical Approval

We affirm that this manuscript is an original work, has not been previously published, and is not currently under consideration for publication in any other journal or conference proceedings. All authors have reviewed and approved the manuscript, and the order of authorship has been mutually agreed upon.

Funding

Not Applicable

Availability of data and material

All of the data obtained or analyzed during this study is included in this paper.

Conflicts of Interest

The authors declare that they have no financial or personal interests that could have influenced the research and findings presented in this paper. The authors alone are responsible for the content and writing of this article.

Author's contribution statement

All authors have contributed equally to the research and preparation of this work.

Data availability statement

The data supporting the findings of this study are available from the corresponding author upon reasonable request.

REFERENCES

[1] Chandrappa, G.T., Steunou, N., Cassaignon, S., Bauvais, C. and Livage, J., **2003**. Hydrothermal synthesis of vanadium oxide nanotubes from V2O5 gels. *Catalysis Today*, *78*(1-4), pp.85-89. https://doi.org/10.1016/S0920-5861(02)00298-5

[2] Menezes, W.G., Reis, D.M., Benedetti, T.M., Oliveira, M.M., Soares, J.F., Torresi, R.M. and Zarbin, A.J., **2009**. V2O5 nanoparticles obtained from a synthetic bariandite-like vanadium oxide: Synthesis, characterization and electrochemical behavior in an ionic liquid. *Journal of colloid and interface science*,

© Ariston Publications 2026. All rights reserved.

337(2), pp.586-593. https://doi.org/10.1016/j.jcis.2009.05.050

[3] Dai, X.C., Hou, S., Huang, M.H., Li, Y.B., Li, T. and Xiao, F.X., **2019**. Electrochemically anodized one-dimensional semiconductors: A fruitful platform for solar energy conversion. *Journal of Physics: Energy*, *1*(2), p.022002. https://doi.org/10.1088/2515-7655/ab0718

[4] Andreozzi, R., Caprio, V., Insola, A. and Marotta, R., **1999**. Advanced oxidation processes (AOP) for water purification and recovery. *Catalysis today*, *53*(1), pp.51-59. https://doi.org/10.1016/S0920-5861(99)00102-9

[5] Deng, J., Jiang, J., Zhang, Y., Lin, X., Du, C. and Xiong, Y., **2008**. FeVO4 as a highly active heterogeneous Fenton-like catalyst towards the degradation of Orange II. *Applied Catalysis B: Environmental*, *84*(3-4), pp.468-473. https://doi.org/10.1016/j.apcatb.2008.04.029

[6] Augugliaro, V., Palmisano, G., Palmisano, L. and Soria, J., **2019**. Heterogeneous photocatalysis and catalysis: An overview of their distinctive features. *Heterogeneous photocatalysis*, pp.1-24. https://doi.org/10.1016/B978-0-444-64015-4.00001-8

[7] Zhou, F., Yan, C., Sun, Q. and Komarneni, S., **2019**. TiO2/Sepiolite nanocomposites doped with rare earth ions: Preparation, characterization and visible light photocatalytic activity. *Microporous and Mesoporous Materials*, *274*, pp.25-32. https://doi.org/10.1016/j.micromeso.2018.07.031

[8] Shen, T.F.R., Lai, M.H., Yang, T.C.K., Fu, I.P., Liang, N.Y. and Chen, W.T., **2012**. Photocatalytic production of hydrogen by vanadium oxides under visible light irradiation. *Journal of the Taiwan Institute of Chemical Engineers*, *43*(1), pp.95-101. https://doi.org/10.1016/j.jtice.2011.06.004

[9] Bagheri, S., TermehYousefi, A. and Do, T.O., **2017**. Photocatalytic pathway toward degradation of environmental pharmaceutical pollutants: structure, kinetics and mechanism approach. *Catalysis Science & Technology*, *7*(20), pp.4548-4569. https://doi.org/10.1039/c7cy00468k

[10] Chen, F., Huang, H., Ye, L., Zhang, T., Zhang, Y., Han, X. and Ma, T., **2018**. Thickness-dependent facet junction control of layered BiOIO3 single crystals for highly efficient CO2 photoreduction. *Advanced Functional Materials*, *28*(46), p.1804284. https://doi.org/10.1002/adfm.201804284

[11] Sajid, M.M., Amin, N., Shad, N.A., Javed, Y. and Zhang, Z., **2019**. Hydrothermal fabrication of monoclinic bismuth vanadate (m-BiVO4) nanoparticles for photocatalytic degradation of toxic organic dyes. *Materials Science and Engineering: B*, *242*, pp.83-89. https://doi.org/10.1016/j.mseb.2019.03.012

[12] Ding, N., Liu, S., Feng, X., Gao, H., Fang, X., Xu, J., Tremel, W., Lieberwirth, I. and Chen, C., **2009**. Hydrothermal growth and characterization of nanostructured vanadium-based oxides. *Crystal Growth and Design*, *9*(4), pp.1723-1728. https://doi.org/10.1021/cg800645c

[13] Sediri, F., Touati, F. and Gharbi, N., **2007**. A one-step hydrothermal way for the synthesis of vanadium oxide nanotubes containing the phenylpropylamine as template obtained via non-alkoxide route. *Materials letters*, *61*(8-9), pp.1946-1950. https://doi.org/10.1016/j.matlet.2006.07.109

[14] Le, T.K., Kang, M. and Kim, S.W., **2019**. Morphology engineering, room-temperature photoluminescence behavior, and sunlight photocatalytic activity of V2O5 nanostructures. *Materials Characterization*, *153*, pp.52-59. https://doi.org/10.1016/j.matchar.2019.04.046

[15] Chirayil, T., Zavalij, P.Y. and Whittingham, M.S., **1998**. Hydrothermal synthesis of vanadium oxides. *Chemistry of materials*, *10*(10), pp.2629-2640. https://doi.org/10.1021/cm980242m

[16] Zhou, F., Zhao, X., Yuan, C. and Li, L., **2008**. Vanadium pentoxide nanowires: hydrothermal synthesis, formation mechanism, and phase control parameters. *Crystal Growth and Design*, *8*(2), pp.723-727. https://doi.org/10.1021/cg060816x

[17] Apostolopoulou, M., Louloudakis, D., Vernardou, D., Katsarakis, N., Koudoumas, E. and Kiriakidis, G., **2015**. Study of the pH effect on the properties of the hydrothermally grown V2O5. *Thin Solid Films*, *594*, pp.338-342. https://doi.org/10.1016/j.tsf.2015.02.056

[18] Avansi Jr, W., de Mendonça, V.R., Lopes, O.F. and Ribeiro, C., **2015**. Vanadium pentoxide 1-D nanostructures applied to dye removal from aqueous systems by coupling adsorption and visible-light photodegradation. *Rsc Advances*, *5*(16), pp.12000-12006. https://doi.org/10.1039/c4ra12788a

[19] Povar, I., Zinicovscaia, I., Spinu, O. and Pintilie, B., **2019**. Thermodynamic stability areas of polyvanadates of alkaline earth metals. *Journal of Chemistry*, *2019*(1), p.7091781. https://doi.org/10.1155/2019/7091781

 © Ariston Publications 2026. All rights reserved.

[20] Shafitri, M., **2019**. Vanadium Pentaoksida (V2O5): Termodinamika Molecular dan Interaksi Ion dalam Larutan.

[21] Povar, I., Spinu, O., Zinicovscaia, I., Pintilie, B. and Ubaldini, S., **2019**. Revised Pourbaix diagrams for the vanadium–water system. *Journal of Electrochemical Science and Engineering*, *9*(2), pp.75-84. https://doi.org/10.5599/jese.620

[22] Liu, B., Yin, D., Zhao, F., Khaing, K.K., Chen, T., Wu, C., Deng, L., Li, L., Huang, K. and Zhang, Y., **2019**. Construction of a novel Z-scheme heterojunction with molecular grafted carbon nitride nanosheets and V2O5 for highly efficient photocatalysis. *The Journal of Physical Chemistry C*, *123*(7), pp.4193-4203. https://doi.org/10.1021/acs.jpcc.8b11361

[23] Aslam, M., Ismail, I.M., Salah, N., Chandrasekaran, S., Qamar, M.T. and Hameed, A., **2015**. Evaluation of sunlight induced structural changes and their effect on the photocatalytic activity of V2O5 for the degradation of phenols. *Journal of hazardous materials*, *286*, pp.127-135. https://doi.org/10.1016/j.jhazmat.2014.12.022

[24] Raible, I., Burghard, M., Schlecht, U., Yasuda, A. and Vossmeyer, T., **2005**. V2O5 nanofibres: novel gas sensors with extremely high sensitivity and selectivity to amines. *Sensors and Actuators B: Chemical*, *106*(2), pp.730-735. https://doi.org/10.1016/j.snb.2004.09.024

[25] Gopinath, R. and Patel, B.K., **2000**. A catalytic oxidative esterification of aldehydes using V2O5− H2O2. *Organic letters*, *2*(5), pp.577-579. https://doi.org/10.1021/ol990383+

[26] Cottineau, T., Toupin, M., Delahaye, T., Brousse, T. and Bélanger, D., **2006**. Nanostructured transition metal oxides for aqueous hybrid electrochemical supercapacitors. *Applied Physics A*, *82*(4), pp.599-606. https://doi.org/10.1007/s00339-005-3401-3

[27] Cheng, K.C., Chen, F.R. and Kai, J.J., **2006**. V2O5 nanowires as a functional material for electrochromic device. *Solar energy materials and solar cells*, *90*(7-8), pp.1156-1165. https://doi.org/10.1016/j.solmat.2005.07.006

[28] Vernardou, D., Spanakis, E., Kenanakis, G., Koudoumas, E. and Katsarakis, N., **2010**. Hydrothermal growth of V2O5 photoactive films at low temperatures. *Materials Chemistry and Physics*, *124*(1), pp.319-322. https://doi.org/10.1016/j.matchemphys.2010.06.040

[29] Gondal, M.A., Hameed, A., Yamani, Z.H. and Suwaiyan, A., **2004**. Production of hydrogen and oxygen by water splitting using laser induced photo-catalysis over Fe2O3. *Applied Catalysis A: General*, *268*(1-2), pp.159-167. https://doi.org/10.1016/j.apcata.2004.03.030

[30] Bickley, R.I. and Jayanty, R.K.M., **1974**. Photo-adsorption and photo-catalysis on titanium dioxide surfaces. Photo-adsorption of oxygen and the photocatalyzed oxidation of isopropanol. *Faraday Discussions of the Chemical Society*, *58*, pp.194-204. https://doi.org/10.1039/DC9745800194

[31] Tan, D., Long, H., Zhou, H., Deng, Y., Liu, E., Wang, S. and Zhang, S., **2020**. Effective photocatalytic degradation of methyl orange using V2O5@ ZnO nanocomposite under UV and visible irradiations. *International Journal of Electrochemical Science*, *15*(12), pp.12232-12243. https://doi.org/10.20964/2020.12.75

[32] Sivarajan, Y., Ishak, K.A. and Yaacob, J.S., **2025**. Green synthesis of tin oxide (SnO2) nanoparticles using ginger extracts for photocatalytic degradation of organic dyes in wastewater. *Applied Biochemistry and Biotechnology*, *197*(9), pp.5668-5693. https://doi.org/10.1007/s12010-025-05293-2

[33] Zeleke, M.A. and Kuo, D.H., **2019**. Synthesis and application of V2O5-CeO2 nanocomposite catalyst for enhanced degradation of methylene blue under visible light illumination. *Chemosphere*, *235*, pp.935-944. https://doi.org/10.1016/j.chemosphere.2019.06.230

[34] Qamar, M. and Muneer, M., **2009**. A comparative photocatalytic activity of titanium dioxide and zinc oxide by investigating the degradation of vanillin. *Desalination*, *249*(2), pp.535-540. https://doi.org/10.1016/j.desal.2009.01.022

[35] Le, T.K., Kang, M. and Kim, S.W., **2019**. Relation of photoluminescence and sunlight photocatalytic activities of pure V2O5 nanohollows and V2O5/RGO nanocomposites. *Materials Science in Semiconductor Processing*, *100*, pp.159-166. https://doi.org/10.1016/j.mssp.2019.04.047

[36] Thi Quan, M.N., Van Lai, D., Tonezzer, M., Do, D.Q. and La, D.D., **2025**. Surfactant-tuned vanadium pentoxide for enhanced photocatalytic degradation of organic dyes: nanosheet vs. microflower morphologies. *RSC advances*, *15*(22), pp.17277-17289. https://doi.org/10.1039/d5ra01050k

[37] Hassan, M.S., Amna, T., Yang, O.B., Kim, H.C. and Khil, M.S., **2012**. TiO2 nanofibers doped with rare earth elements and their photocatalytic activity. *Ceramics International*, *38*(7), pp.5925-5930. https://doi.org/10.1016/j.ceramint.2012.04.043

© Ariston Publications 2026. All rights reserved.

[38] Vernardou, D., Drosos, H., Fasoulas, J., Koudoumas, E. and Katsarakis, N., **2014**. Photocatalytic properties of chemically grown vanadium oxide at 65° C. *Thin Solid Films*, *555*, pp.169-172. https://doi.org/10.1016/j.tsf.2013.05.144

[39] Xiong, C., Aliev, A.E., Gnade, B. and Balkus Jr, K.J., **2008**. Fabrication of silver vanadium oxide and V_2O_5 nanowires for electrochromics. *ACS nano*, *2*(2), pp.293-301. https://doi.org/10.1021/nn700261c

[40] Zhang, M., Li, Y. and Shen, Z., **2019**. "Water-in-salt" electrolyte enhanced high voltage aqueous supercapacitor with all-pseudocapacitive metal-oxide electrodes. *Journal of Power Sources*, *414*, pp.479-485. https://doi.org/10.1016/j.jpowsour.2019.01.037

[41] Gopinath, R., Barkakaty, B., Talukdar, B. and Patel, B.K., **2003**. Peroxovanadium-catalyzed oxidative esterification of aldehydes. *The Journal of Organic Chemistry*, *68*(7), pp.2944-2947. https://doi.org/10.1021/jo0266902

[42] Modafferi, V., Panzera, G., Donato, A., Antonucci, P.L., Cannilla, C., Donato, N., Spadaro, D. and Neri, G., **2012**. Highly sensitive ammonia resistive sensor based on electrospun V2O5 fibers. *Sensors and Actuators B: Chemical*, *163*(1), pp.61-68. https://doi.org/10.1016/j.snb.2012.01.007

[43] Jiang, D., Ma, W., Xiao, P., Shao, L., Li, D. and Chen, M., **2018**. Enhanced photocatalytic activity of graphitic carbon nitride/carbon nanotube/Bi2WO6 ternary Z-scheme heterojunction with carbon nanotube as efficient electron mediator. *Journal of Colloid and Interface Science*, *512*, pp.693-700. https://doi.org/10.1016/j.jcis.2017.10.074

[44] Zhou, X., Wei, C., Li, M., Qiu, S. and Li, X., **2011**. Thermodynamics of vanadium–sulfur–water systems at 298 K. *Hydrometallurgy*, *106*(1-2), pp.104-112. https://doi.org/10.1016/j.hydromet.2010.12.003

[45] Artika, P.I. and Zainul, R., **2018**. Potassium Bromide (KBr): Transformasi ionik dan sifat temodinamika dalam Larutan.

[46] Volkov, V.L. and Podval'naya, N.V., **2000**. Phase composition and formation kinetics of polyvanadates in the KVO_3-$VOSO_4$-K_2SO_4-H_2O system.

[47] Potiron, E., Salle, A.L.G.L., Guyomard, D. and Piffard, Y., **1998**. Synthesis, Characterization and lithium Intercalation behavior of electrodeposited V_2O_5. *Molecular Crystals and Liquid Crystals Science and Technology. Section A. Molecular Crystals and Liquid Crystals*, *311*(1), pp.75-80. https://doi.org/10.1080/10587259808042369

[48] Li, G., Chao, K., Peng, H., Chen, K. and Zhang, Z., **2007**. Low-valent vanadium oxide nanostructures with controlled crystal structures and morphologies. *Inorganic chemistry*, *46*(14), pp.5787-5790. https://doi.org/10.1021/ic070339n

[49] Nazar, L.F., Koene, B.E. and Britten, J.F., **1996**. Hydrothermal Synthesis and Crystal Structure of a Novel Layered Vanadate with 1, 4-Diazabicyclo [2.2. 2] octane as the Structure-Directing Agent:($C_6H_{14}N_2$) $V_6O_{14}.H_2O$. *Chemistry of materials*, *8*(2), pp.327-329. https://doi.org/10.1021/cm9504302

[50] Kianfar, E., Baghernejad, M. and Rahimdashti, Y., **2015**. Study synthesis of vanadium oxide nanotubes with two template hexadecylamin and hexylamine.

 © Ariston Publications 2026. All rights reserved.